Flat plate pressure impact on a still water surface: The effect of surrounding ambient pressure and plate size

Abdessamad Talioua, Belaïd Berkane, Marc Batlle Martin, Gaële Perret, Grégory Pinon

Ocean Engineering 263 (2022) 111926

Contents lists available at ScienceDirect

Ocean Engineering

journal homepage: www.elsevier.com/locate/oceaneng

Flat plate pressure impact on a still water surface: The effect of surrounding ambient pressure and plate size

Abdessamad Talioua [a], Belaïd Berkane [a], Marc Batlle Martin [b,c], Gaële Perret [a], Grégory Pinon [a,*]

[a] Normandie Univ, UNILEHAVRE, UMR 6294 CNRS, LOMC 76600 Le Havre, France
[b] France Energies Marines, Plouzané, Bretagne, France
[c] Laboratoire d'Hydraulique Saint-Venant, EDF R&D, Chatou, France

ARTICLE INFO

Keywords:
Fluid–structure impact
Slamming
Impact pressure
Pressure–impulse
Cushion effect

ABSTRACT

The study of the impact between a rigid structure and water has raised the interest of many researchers in these recent years. This problem is relevant to various engineering applications, and particularly in the nautical environment (renewable energy, marine applications...). The present paper details an experimental investigation of rigid circular plates impacts into pure water. The analyses are based on impact pressure temporal signals, pressure impulses and frequency analysis recorded while the plates were impinging the still water surface. The measurement campaigns were carried out at the University Le Havre Normandy's LOMC laboratory, in a recently developed experimental facility. In the previous experimental and numerical studies, it was observed that the magnitude of the peak slamming pressure is reduced if compared to the theoretical model predicted by von Karman (1929). Similar observations were made here and the decrease was partly attributed to the cushion effect resulting from the presence of an entrapped air layer between the rigid plate and the water free surface. This work aims to study the influence of the cushion effect on the impact pressure by using four rigid circular plates with different diameters in order to modify the volume of the air layer. Initially, the measurements were carried out for an ambient pressure equal to the atmospheric pressure. In a second part of the study, the same measurements were performed for two lower ambient pressures (about 75% and 50% of the atmospheric pressure) in order to minimise the cushion effect. And finally, a frequency analysis is presented with comparisons to theoretical results of Minnaert (1933) in order to correlate the air layer size to the pressure oscillation characteristics. The obtained results were compared with previous experimental and theoretical studies for low impact velocities ($V \leq 1.2$ m/s).

1. Introduction

When a fluid strikes a body, very large forces are generated over a very short period of time. This hydrodynamic situation is observed in several fields ranging from sea wave loads or direct impact of hulls with the free surface. The coastal and offshore structures also face such conditions during breaking waves impingement. Moreover, the phenomenon has also been widely investigated during sloshing conditions, i.e., when a partly filled liquid tank undergoes a rolling situation and causes breaking waves impacts on the tank internal walls. Another example of a fluid solid impact is observable during an aircraft emergency ditching or in nautical sports when athletes jump into water from considerable heights. In order to participate to increasing global understanding of solid–fluid impacts, this paper will be dedicated to flat circular plate impinging on a still water surface.

In order to get a detailed understanding of water–structure impacts, the phenomenon has been investigated using experimental, theoretical and numerical approaches for several decades. To clarify the properties of water slamming, these studies are based on the analysis of pressure and the impulse during the impact. To the best of the author's knowledge, this phenomenon was initially observed during a documentation of wave loading on caisson breakwaters in 1840 by Stevenson (1840) on site at Dunbar, a UK harbour. The first theory to estimate the maximum pressure during a fluid impact was developed by von Karman (1929) while studying the problem of a seaplane ditching commonly called the water entry problem. In his work, it was found that the peak pressure during a flat bottom solid impact on a compressible liquid was equal to the acoustic pressure $P_{max} = \rho V c$, where ρ is the fluid density, V is the velocity at the instant of impact and c the speed of sound in the fluid. Even though this was not the main objective of the numerical study published by Braeunig et al. (2009), some very interesting insights toward the validation of the von Karman theory can be

* Corresponding author.
E-mail address: gregory.pinon@univ-lehavre.fr (G. Pinon).

https://doi.org/10.1016/j.oceaneng.2022.111926
Received 4 February 2022; Received in revised form 27 May 2022; Accepted 3 July 2022
Available online 29 August 2022

found in that study. In fact, Braeunig et al. studied liquid impact using a two-phase finite volume compressible solver to investigate the loads exerted on a horizontal plane by a free-falling block. And by decreasing the air density close to zero, mimicking a water impact in the void, the obtained impact pressures by Braeunig et al. were approaching this von Karman's theory. The work presented in the current paper aims at assessing if one can validate this von Karman's theory with an experimental device, by reproducing the Braeunig et al.'s configuration: a water impact in the void. From another perspective, also following the von Karman theory $P_{max} = \rho V c$, the dependency of the pressure maximum to the liquid speed of sound c could also explain the great variability of the pressure magnitude depending on the fluid. In fact, in the study of Wood (1941), the sound speed was analysed for different mixtures of air and water and it was observed that for an air volume fraction of 1%, the speed of sound decreased to $\approx$ 200 m/s. This would imply a drastic decrease of the impact pressure (when using the acoustic pressure theory) in the case of slightly aerated sea water when compared to a pure liquid situation where the speed of sound is $\approx$ 1500 m/s. In the present paper and to start with, only pure water impacts will be presented and discussed.

For real life configurations, the on-site wave loads records on the breakwater of Dieppe by de Rouville et al. (1938) reported a great spatial and temporal variability of the pressure signals by apparently similar waves. This motivated the study of Bagnold (1939) to perform laboratory controlled breaking waves and investigate the impact pressure fields exerted on a vertical wall. In his work, Bagnold pointed out the important role of air being entrapped between the overturning wave and the solid surface during an impact, which produces a non-negligible cushioning effect. Regarding the water entry problem, this effect is also likely to occur by entrapping air between the solid and the free surface. This effect was not taken into account in the theoretical work of von Karman. However, von Karman's work was extended theoretically and experimentally by Verhagen et al. (1967) by assuming a deformation of the free surface before the impact which consequently entrapped an air layer. The air entrapment is especially relevant when the model makes use of a flat bottom solid (see e.g. Chuang et al., 1966; Verhagen et al., 1967; Lewison et al., 1968) rather than a wedge-shaped solid (see e.g. Chuang, 1966; Zhu, 1995; Zhao et al., 1997). In the experiments of Chuang et al. (1966) using a flat plate, the maximum impact pressure was found to be proportional to the acoustic pressure in the air (i.e. using the speed of sound in air) due to the aforementioned air cushioning effect. These experiments were carried out at relatively low velocities of the solid $V < 1.92$ m/s, a velocity range similar to the one experimented here. Hattori et al. (1994) further investigated the air cushioning effect by performing experiments of a breaking wave impact on a vertical wall. This study reported that the impact pressure magnitude increased when reducing the amount of air being entrapped between the liquid and the solid; and also related the appearance of pressure oscillations to the compression and expansion of the air cavity during the impingement.

Recently, Lugni et al. (2010b,a) employed a sloshing tank experimental setup for recreating breaking waves conditions and measured the related pressure loads. In this work, the objective was to study the effect of a depressurisation of the tank on the evolution of the air cavity entrapped during a wave impact. It was reported that by depressuring the tank, the ratio A_{exp}/A_{comp} of the air cavity entrapped area at the instants of maximum expansion A_{exp} and compression A_{comp} drastically increased. It was also pointed out the possible occurrence of cavitation during the cavity compression and expansion pressure fluctuations. As mentioned above, such a depressurisation was also studied numerically by Braeunig et al. (2009). In fact, diminishing the air density (to a very low value) can be considered as depressurising the tested flow configuration. Therefore, three ambient pressure configurations will be tested in the present experimental campaign, one close to atmospheric pressure and two with increasing depressurisation in order to possibly reproduce Braeunig et al.'s configurations.

The numerical work of Ma et al. (2014) investigated the water entry problem into pure and aerated water. In their work, it was reported a reduction of the pressure peak and an increase of the rise times (i.e. the interval since the pressure increases until the maximum peak) when increasing the liquid aeration. Moreover, it was reported the presence of shock waves, travelling through the liquid phase, that arises the liquid compressibility. Other numerical studies explored the fluid compressibility from different fluid impact perspectives e.g. Guilcher et al. (2010), Ma et al. (2016), Gatin et al. (2020), Batlle Martin et al. (2021) among others. The reduction of the pressure peak due to the presence of entrapped air was initially reported experimentally by Bullock et al. (2001) and it has been recently confirmed using a flat plate water entry experiments for velocities of the solid ranging from $1 - 7$ m/s by Mai et al. (2019). In the present paper, after analysing the obtained experimental results, the importance of such an entrapped air bubble is investigated in order to be further characterised. Even though the velocity range ($V \leq 1.2$ m/s here) is smaller than the one of Mai et al., it is still in the range of experimentally observed one at the laboratory scale. In fact, in the work of Kimmoun et al. (2009) where solitary waves were impinging a flat wall, some PIV measurements were performed where a velocity of 1.2 m/s was measured for highly impulsive impacts. These velocity fields were reproduced in Lu et al. (2021) and Batlle Martin et al. (2021) for instance. And the objectives of Kimmoun et al.'s work was clear: study, at the laboratory scale, the maximum impact pressures in Liquefied Natural Gas tankers representative of real impact configurations.

The aim of the present work is first to assess, via an academic test configuration, whether the von Karman (1929)'s theory can be reproduced experimentally. For this, three ambient pressure configurations are tested aiming to reproduce experimentally the numerical configurations of Braeunig et al. (2009). Of course, different plate diameters and impact velocities will be considered. Therefore, the paper is divided as follows. Section 2 describes the experimental setup, the experimental protocol and the measurement techniques validation. This section summarises details of the method used to determine the peak slamming pressure and the pressure impulse. Then, Section 3 presents and analyses the obtained results of the maximum impact pressures and pressure impulses for ambient atmospheric pressure configurations. The following Section 4 analyses similar results but for sub-atmospheric configurations. And the last Section 5 details a frequency analysis carried out for all the above-mentioned configurations. Finally, some conclusions are drawn as well as perspectives for future work are discussed in Section 6.

2. Methodology

2.1. Experimental set-up

Impact pressure of solid plates impinging on a flat water surface has been studied by means of an experimental set-up recently developed at the University Le Havre Normandy. The experimental set-up is given in Fig. 1. Different circular 10 mm-thick steel plates of diameters $D =$ 3 cm, 6 cm, 10 cm and 14 cm were used. The tank is 52.5 cm long by 47.5 cm wide and 55.3 cm deep, made of 12 mm thick PMMA panels. Considering a sound velocity in water about 1450 m/s, the tank's dimensions lead to natural frequencies, *i.e* frequencies related to the reflection of the acoustic wave between the tank walls, of 2762 Hz, 3053 Hz and 1686 Hz (see Section 5 for more details). Those frequencies are much higher than the observed oscillating frequencies of the air cushion trapped below the plates. For these experiments, the tank is filled with demineralised water to a height of $h = 43$ cm. The impact pressure was measured using a Kistler piezoelectric PE pressure sensor of type 601CAA of diameter 5.55 mm. Pressure signals are recorded using the software provided by Kistler with a DC amplifier with an acquisition frequency up to a maximum of 208 333 Hz. The circular plates are screwed around the sensor, i.e., the impact pressure

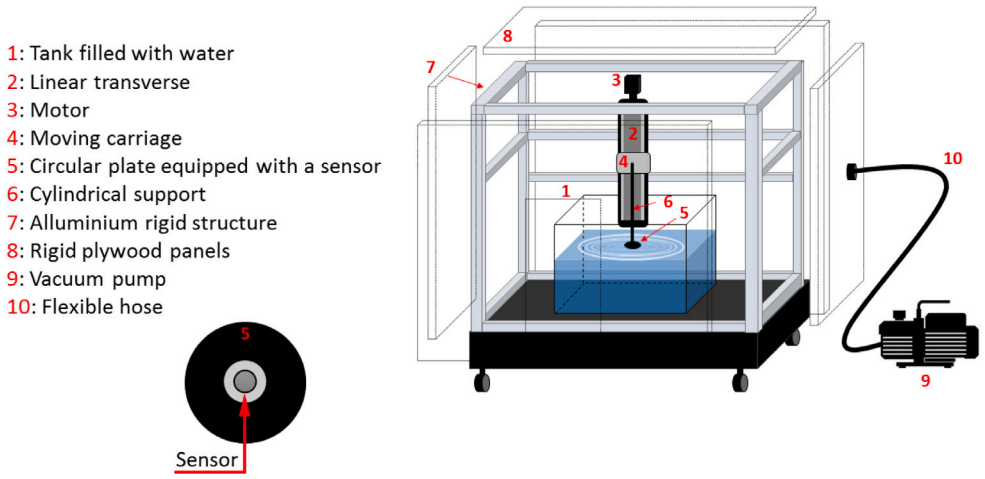

Fig. 1. Experimental set-up.

is measured at the centre of each plate, where the impact pressure is supposed to be the greatest (Mai et al., 2019). The sensor itself is screwed on a cylindrical support connected to a carriage moving vertically at a constant velocity on a motorised linear transverse system (Zaber X-LRT0750DL-E08C). The carriage can move over a distance of 75 cm, where the motor is controlled via Zaber Console software. Due to the short distance to be crossed by the carriage as well as to the power of the motor, the maximum travelling speed (i.e. the maximum impact velocity) is limited to 1.2 m/s in this study. For each velocity, the impact moment corresponds to the instant where the carriage is in the middle of the linear transverse. The velocity is thus ensured to be constant at the impact.

For this study, series of measurements were carried out with different ambient pressures: $P_0 \approx 0.5$ bar, 0.75 bar with an error of ± 0.005 bar and 1.015 bar with an error of ± 0.01 bar. To perform this, the whole set was placed inside a sealed enclosure (see Figs. 1, 2). This enclosure was made of rigid plywood panels with a thickness of 18 mm, supported by a structure of 45 mm × 45 mm aluminium sections. In order to promote optical observations as well as access to the interior, an entrance is kept that can be locked up by another plexiglass panel with a thickness of 18 mm, surrounded by a rubber gasket to ensure the tightness during the depression. The distance between the plywood walls and the tank is at least 10 cm. Thus the outer enclosure and the tank are disconnected during depressurisation except on the bottom where a plywood plane ensures the interface between the steel bottom of the structure and the PMMA tank. In order to achieve the depression, a vacuum pump (BECKER U 4.70 SA/K) was used characterised by a flow rate between 70 and 84 m^3/h. To control the ambient pressure inside the enclosure, the vacuum pump is equipped with a valve, which is monitored in real time using a pressure sensor (VEGABAR 38) characterised by a ceramic measuring cell with an accuracy of 0.3%. This sensor is connected to the interior and equipped with a text display allowing the reading of the ambient pressure and temperature values.

2.2. Experimental protocol

In this study, seven impact velocities varying from 0.4 to 1.2 m/s were chosen for each of the three ambient pressures. Also, the four different plate sizes (with D ranging from 3 cm to 14 cm) were systematically studied for each ambient pressure and travelling velocity. For each impact velocity, five acquisitions were recorded in order to verify the results reproducibility. The pressure is thus obtained as the averaged value and the uncertainties correspond to the standard deviation. In between two acquisitions the waiting time is around ten minutes, which is sufficient to guarantee the stabilisation of the water free surface after impacts. The recording always starts before starting

Fig. 2. Photo of the experimental set-up, inside the sealed enclosure.

the displacement of the carriage and stops when the carriage reaches the end position. This measurement campaign was carried out in an ambient temperature of $T = 19 \pm 2$ °C.

2.3. Test validation

In order to study the reliability of the results, a convergence study on the pressure probe acquisition frequency is first performed. The acquisition frequency is varied from 10 Hz and 208 333 Hz, which are the minimum and the maximum frequency of the sensor respectively, for $D = 6$ cm and $V = 1.0$ m/s. For each acquisition frequency, the peak pressure, corresponding to the maximum of pressure time evolution (Fig. 3(b)), is measured. Fig. 3(a) shows that the convergence is obtained for an acquisition frequency larger than ≈ 100 kHz with a standard deviation lower than 2%. However, the maximum frequency of 208 333 Hz has been chosen for the pressure sensor for all the acquisitions presented in the following.

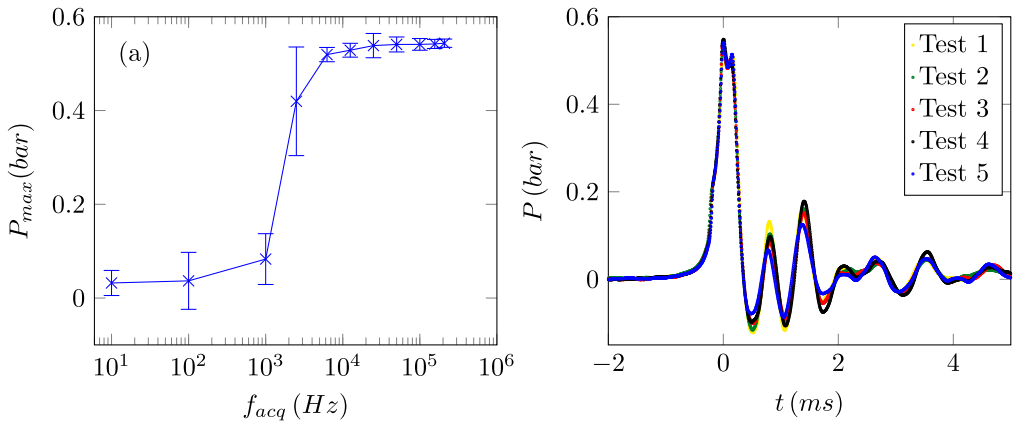

Fig. 3. (a) Convergence of P_{max} measurements as a function of the acquisition frequency, (b) Reproducibility of pressure measurements: five tests of pressure time histories in the same conditions $V = 1$ m/s and $D = 6$ cm.

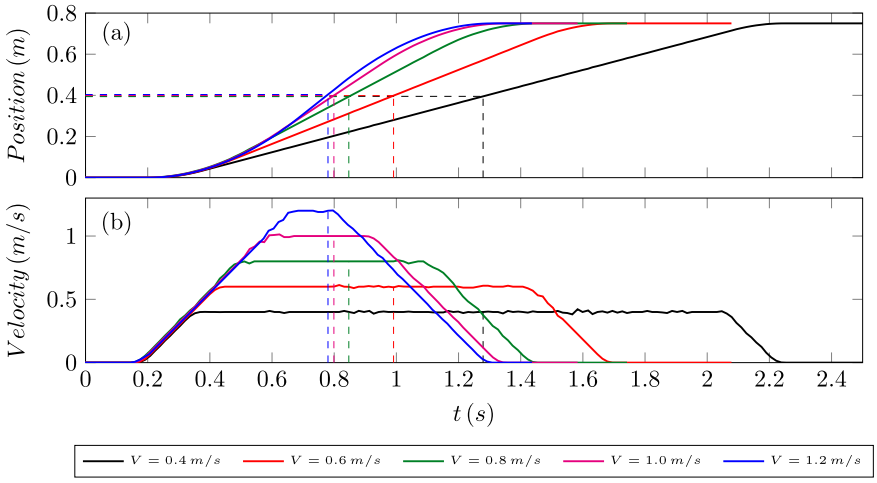

Fig. 4. Typical time histories of the carriage's displacement (a) and velocity (b). The instant of impact is indicated with a vertical dashed line on each of the graph.

Then, the reproducibility of maximum pressure value was verified by reproducing five times the experiments for each given plate's diameter and slamming velocity. Fig. 3(b) depicts the comparison of the temporal signals for five acquisitions. This figure shows that the reproducibility is verified, with a low standard deviation estimated at 2%.

Finally, the impact velocity, i.e. the velocity at which the plate is travelling when it first impacts the water free surface, is presented and discussed. Fig. 4 illustrates the temporal evolution of the carriage position and its velocity for different velocity commands. The impact instant corresponds to the moment when the carriage position arrives at 40 cm, close to the middle of the linear transverse. The velocity at the moment of impact is thus located in the middle of the velocity plateau. Moreover, the nominal speed value given by the software corresponds to the value of the average velocity of the plateau with an uncertainty estimated at around 1%, corresponding to the standard deviation for the five acquisitions.

2.4. Experimental pressure–impulse determination

In the case of this study, a layer of air remains entrapped between the rigid plate and the water free surface. This cushion effect therefore influences the amplitude and the duration of the peak slamming pressure. In particular, the maximum pressure does not evolve linearly with the size of the plate. The duration of the peak must also be taken into account as it will be presented in Sections 3 and 4. The pressure–impulse thus appears to be more adapted to quantify the impact. This pressure–impulse is defined as follows:

$$I = \int_{t_i}^{t_f} P(t)\,\mathrm{d}t$$

where t_i *and* t_f are the initial and final time of the impact respectively. For the calculation, a common criterion is defined for all cases of this study. The initial time t_i is defined as the instant when $dp(t)/dt$ becomes larger than 110 Pa s^{-1}. This arbitrary threshold appears to be consistent with all the measurements. An example is presented in Fig. 5(a). The final time t_f is estimated by taking the first intersection of the pressure time signal with the axis $P = 0$ *bar* after the impact. This method is shown in Fig. 5(b). Finally, the pressure–impulse corresponds to the integral of the area shown in colour (see Fig. 5(b)).

3. Results at ambient atmospheric pressure

3.1. Maximum pressure evolution with impact velocity

Fig. 6 shows the maximum pressure against the impact velocity for the different plate diameters and all tested impact velocities.

Experimental data is compared with theoretical predictions from von Karman (1929) and the semi-analytical formula from Chuang (1966). Not surprisingly, maximum measured pressures are much lower than the acoustic pressure estimated by von Karman. This difference is most probably due to the air layer entrapped between the plates and the water-free surface at the moment of the first contact which induces an air cushion effect. Based on experimental observations of a falling plate

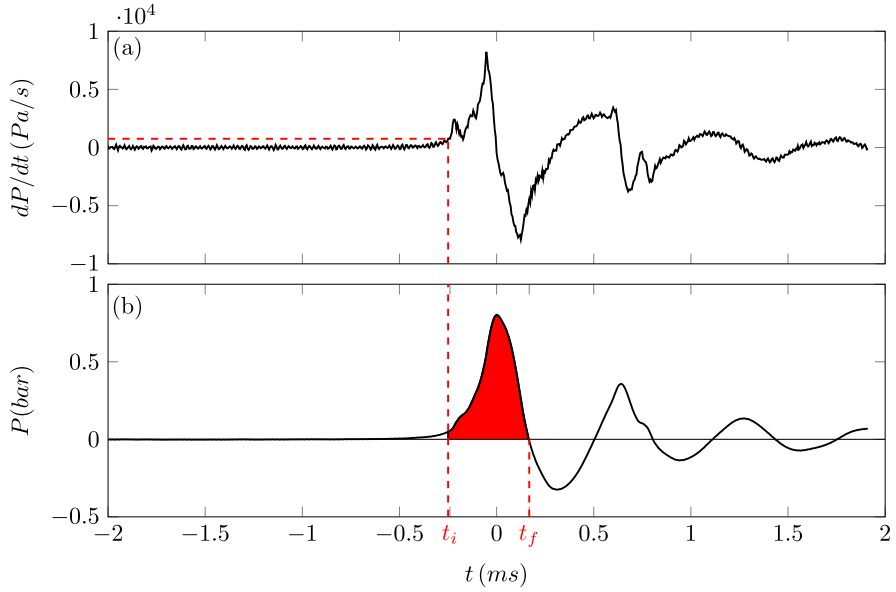

Fig. 5. (a) Derivative of typical pressure time histories, (b) typical pressure time histories with coloured area representing the pressure impulse (I). (For interpretation of the references to colour in this figure legend, the reader is referred to the web version of this article.)

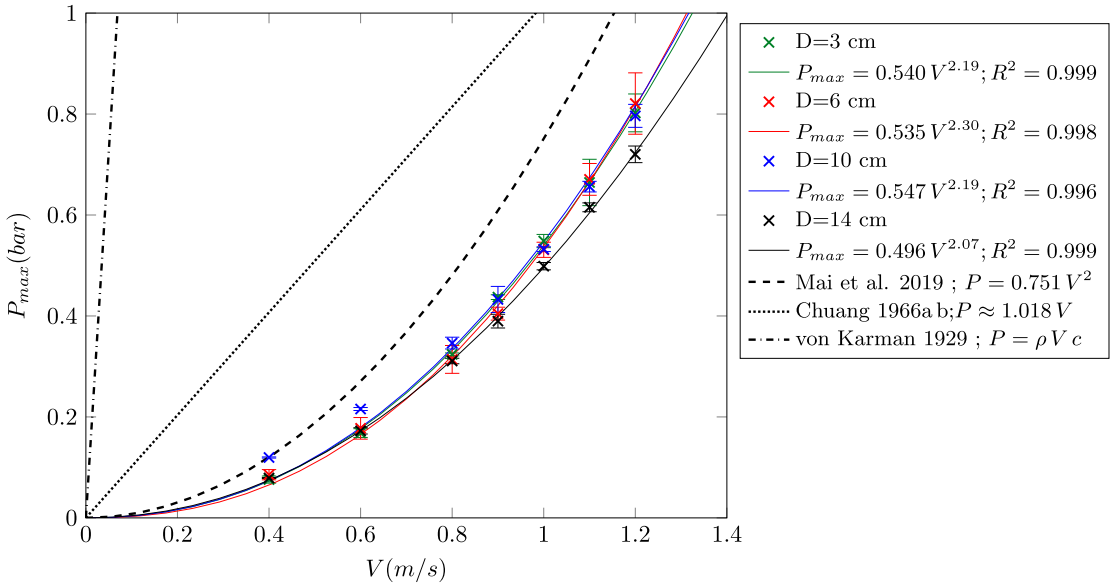

Fig. 6. Impact pressure as a function of impact velocity for different plate's size at ambient pressure $P_0 = 1.015\,bar$.

and theoretical reasoning, Chuang (1966), Chuang et al. (1966) found a linear law for impact velocity $V \leq 1.92$ m/s. However, Chuang's law also overestimates the maximum measured pressure. Indeed, in the present study, the power law evolution of the peak pressure with impact velocity is close to 2 for all the plates. These results are confirmed by the recent study from Mai et al. (2019) for impact velocities 2 m/s $\leq V \leq$ 7 m/s. The solid lines in Fig. 6 represent the fitted curves for each case obtained using the non-linear least-square algorithm in Matlab. It has been found that the maximum pressure is proportional to the square of impact velocity: $P \approx A V^2$, where A is an empirical coefficient estimated using the curve fitting tool.

Although the peak pressure increases with slamming velocity for all the plates, it does not necessarily increases with the size of the plate at a given velocity as it could be expected. As a matter of example, for $V = 1.2$ m/s, the maximum pressure P_{max} is $0.820\,bar$ for $D = 6$ cm, $0.796\,bar$ for $D = 10$ cm and $0.720\,bar$ for $D = 14$ cm. Therefore, based on the presented results, no clear conclusion can be drawn on the behaviour of the plate's size yet. However, the presence of the air cushion effect could be evoked from the results presented in Fig. 7, which compares typical time histories of the pressure for all diameters for $V = 1.2$ m/s, $V = 0.9$ m/s and 0.4 m/s in the case of an ambient pressure of $P_0 = 1.015\,bar$.

The instant $t = 0$ s is chosen as the time of the peak slamming pressure; i.e., the maximum pressure. In general, the evolution of the pressure signals consists of three stages: the peak slamming pressure corresponding to the impact phenomenon between the circular plate and the water free surface, a rapid decrease in pressure due to the fluid expansion, and post-impact oscillations. The different steel plates being 10 mm thick, the plate elasticity was supposed to be negligible and the rigidity of the whole assembly as nearly infinite, following the experimental setup description presented in the above section. As shown in Fig. 7 the impact duration increases with the size of the plate. For instance, the duration of the shock is less than 0.2 ms, 0.37 ms, 0.5 ms and 1.1 ms for $D = 3$ cm, $D = 6$ cm, $D = 10$ cm and $D =$

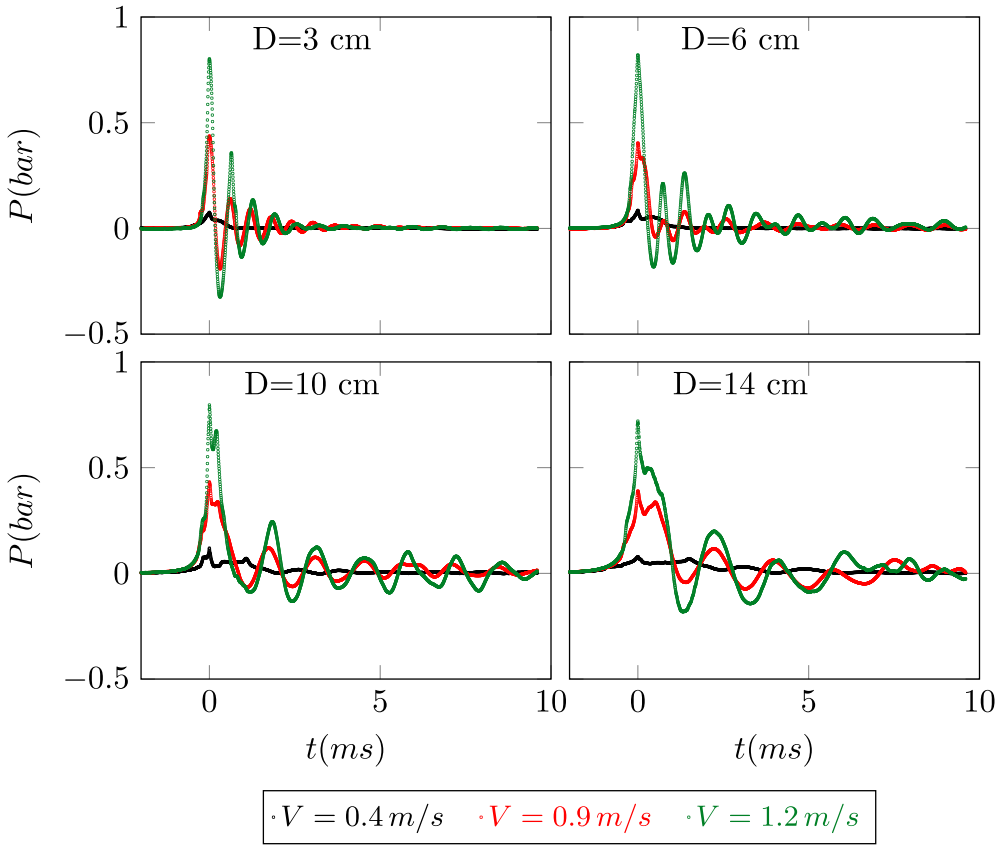

Fig. 7. Typical pressure time histories for different impact velocities V and plate diameters D.

14 cm respectively. Ma et al. (2016) found that the duration of the shock is around 2 ms by using a plate with larger dimensions. These results are consistent as the size of the air layer entrapped between the plate and the water free surface increases with the size of the plate. Moreover, in the last stage of the pressure signals time, the duration of the post-impact oscillations becomes longer as the diameter of the plate is higher, which implies that the quantity of air entrapped becomes higher too. Thus, the pressure impulse which takes into account the maximum pressure and the impact duration, could be more relevant to characterise impact phenomena.

3.2. Pressure impulse evolution with impact velocity

Fig. 8 (left) shows the pressure impulse evolution calculated between the instant when the pressure signal starts to rise up to the peak and then falls down to zero. Details on pressure impulse calculation is presented in Section 2.4. Pressure impulse is found to increase with the impact velocity as well as the size of the plate. This result is therefore consistent with the previous discussion. It was shown in Fig. 7 that the duration of the shock is longer as the diameter of the plate is higher even if the peak is less intense. The second figure (on the right-hand side) shows the dimensionless pressure impulse $I/(P_0.D.V^{-1})$. As it is clearly visible, the curves are superimposed except in the case of the smallest plate ($D = 3$ cm). This could be explained by the weaker cushioning effect in this case compared to other cases (higher D).

To wrap up the findings from this section, several partial conclusions could be drawn. First, even though the very high acquisition frequency enables the observation of the very first instants of impact, the von Karman theory presenting an impact scaling with $\rho V c$ could not be evidenced experimentally. However, in most cases, the maximum impact pressures decrease with increasing the flat plate size and the impact duration increases. Assessing the pressure impulses shows that the obtained results are coherent. An explanation of these results could come from the presence of entrapped air between the flat plate and the still water surface, creating the so-called air cushion effect. This conclusion could also be supported by the pressure oscillations in the signal whose evolution is coherent with the presence of such an air layer. In order to study the effect of the quantity of air entrapped between the plate and the water-free surface on the peak slamming pressure, campaigns of measurements were made with an ambient depressurisation. Hopefully, if the cushion effect could be totally erased by diminishing enough the presence of air, maybe the results could tend to the von Karman theory as numerically obtained by Braeunig et al. (2009). This will be discussed in the following section.

4. Results at sub-atmospheric pressure

4.1. Maximum pressure evolution with impact velocity

The evolution of impact pressure as a function of the impact velocity and plate diameter is studied here for different ambient sub-atmospheric pressures P_0.

From Fig. 9 and as in the previous section, the impact pressure always increases with impact velocity whatever the ambient pressure is. Then, for each diameter taken individually (each of the four plots), the impact pressure increases by decreasing the ambient pressure. This result seems consistent as reducing the ambient pressure means reducing the surrounding air quantities, hence inducing a reduction of cushioning effect as the air entrapped layer between the plate and the water free surface is smaller. Looking closer to the results, one can see only a small increase for the results obtained at $P_0 = 0.75\,bar$ when compared to those of the previous section at $P_0 = 1.015\,bar$. On the contrary, a large increase is obtained for the impact pressure recorded at $P_0 = 0.5\,bar$ with respect to the two other series obtained at higher ambient pressure, except for $D = 3$ cm. As expected, such a depressurisation seems to have had an important effect on the obtained

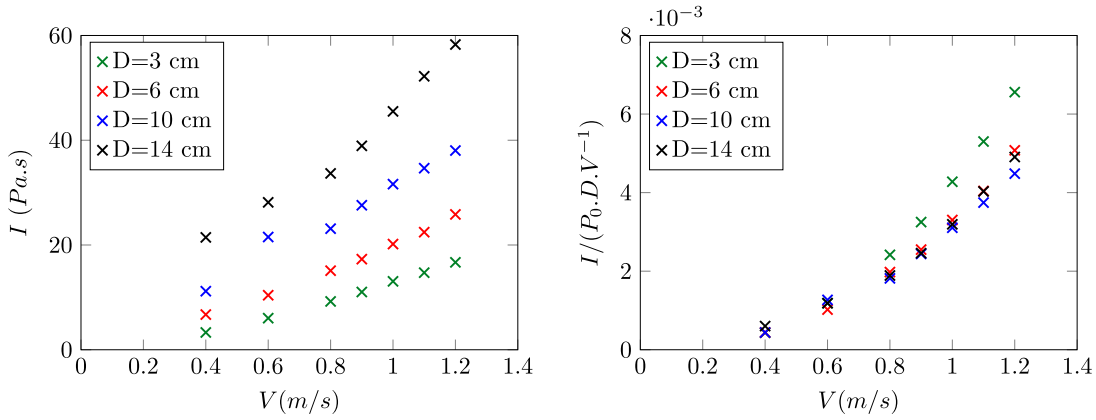

Fig. 8. Pressure impulse as a function of V for $P_0 = 1.015\,bar$.

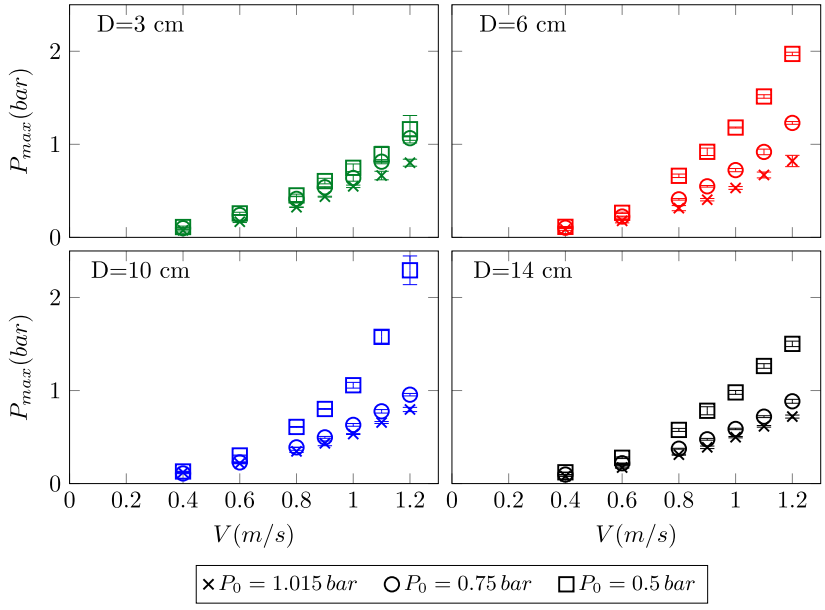

Fig. 9. Maximum pressure evolution as a function of impact velocity for different plate diameters and different atmospheric pressures. Mean and standard deviation values are obtained for the five repeated acquisitions performed for each configuration.

impact pressures. These results are in accordance with the numerical results obtained by Braeunig et al. (2009) by varying the ratio of density between air and water. A similar tendency is obtained and the maximum impact pressures have largely increased. Three observations can be made:

- According to the presented graphs, the maximum pressure is obtained for the two intermediate plate diameters (D = 6 cm and 10 cm), the highest value being for the latter. However, for D = 14 cm the maximum impact pressure values are always lower than for D = 6 cm and 10 cm at $P_0 = 0.5\,bar$. It is as if the depressurisation was not strong enough and, this plate being the larger, a cushioning effect is still well efficient even at this lower ambient pressure value. There should be a relation like: the larger the plate size, the stronger the depressurisation needs to be to diminish the cushioning effect.
- On the contrary, for D = 3 cm, the impact pressures at $P_0 = 0.5\,bar$ only show a very small increase with respect to two other series at $P_0 = 0.75\,bar$ and $P_0 = 1.015\,bar$. For this plate size, it is as if the cushioning effect was not really acting or, its influence being less important when compared to higher plate diameters, this cushioning effect was not really altered by the current values of depressurisation. This was somehow already observable on pressure–impulse results presented in Fig. 8 from previous section.
- Even for the highest depressurisation experienced here ($P_0 = 0.5\,bar$), the results do not scale with the theoretical acoustic pressure predicted by von Karman (1929) with $P_{max}^{theo} \sim \rho V c$. Unfortunately, $P_0 = 0.5\,bar$ ambient pressure reached here is the minimum achievable with the current installation. Additional modifications will be required to the experimental device to go beyond this value. In the future, the authors plan to carry out new measurements for smaller ambient pressures by keeping the same impact conditions.

However, additional post treatments are already possible on the current results and presented in the following. Fig. 10(a) depicts the maximum pressure evolution as a function of the Euler number, defined as $Eu = P_0/(1/2\rho V^2)$. From this graph, one can see a remarkable scaling of the maximum pressure impact as a function of $1/Eu$ with an regression coefficient of $R^2 = 0.96$. Following these results, it is clear that the theoretical scaling of von Karman (1929) with $P_{max}^{theo} \sim \rho V c$ is not achieved. And for all the studied cases, the maximum impact pressure still scales with ρV^2 modified by the ambient pressure P_0. This representation of the results is in accordance with the aforementioned

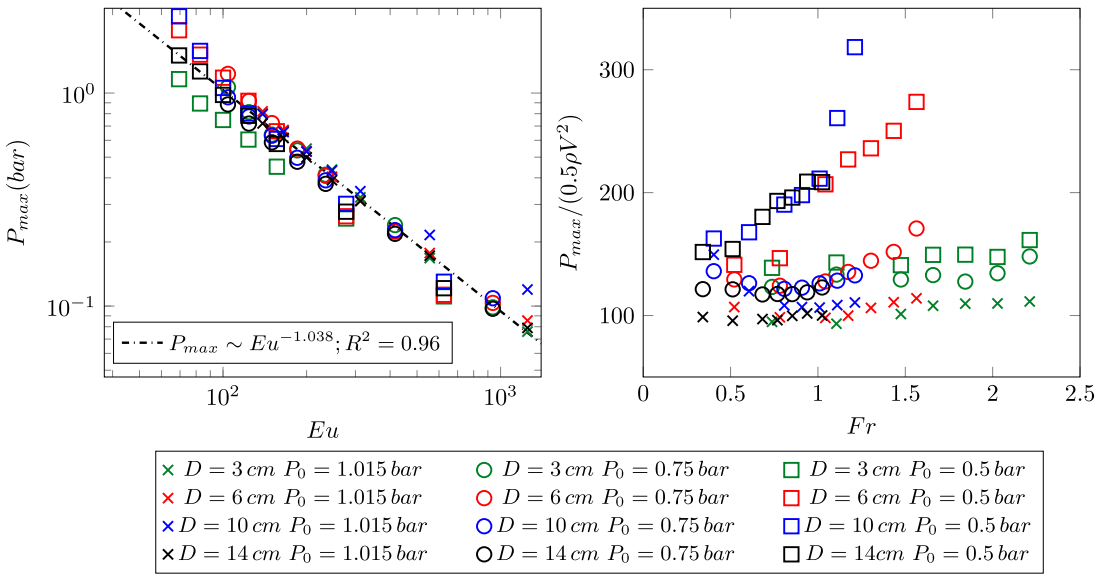

Fig. 10. Maximum pressure as a function of Euler number: $P_0/(1/2\rho V^2)$ (a) and dimensionless maximum pressure as a function of the Froude number $Fr = V/\sqrt{gD}$ (b).

analysis. And if von Karman (1929)'s scaling is expected, a much stronger depressurisation may be needed to achieve so.

However, even if the scaling with $1/Eu$ is quite accurate, most of the values obtained at $P_0 = 0.5\,bar$ are slightly out of the scaling. Fig. 10(b) attempts to give further insights for explaining this behaviour. In fact, Fig. 10(b) depicts the normalised pressure values $P_{max}/(1/2\rho V^2)$ with respect to the Froude number, defined here as $Fr = V/\sqrt{gD}$. From this graph, one can see that $P_{max} \sim 1/2\rho V^2$ for nearly all cases recorded at atmospheric pressure (crosses of all colours in Fig. 10(b)). The observed constant is close to 100 and there is barely no variation with respect to the Froude number. For the case with $D = 3$ cm at the two depressurised values, a similar trend is observed: no variation with the Froude but with a higher constant value. However, for the lowest depressurisation configurations ($P_0 = 0.5\,bar$) for $D = 6$ cm, 10 cm and 14 cm, another scaling is found showing an important modification in the physical phenomenon. In fact, $P_{max}/(1/2\rho V^2)$ seems to linearly increase with increasing Froude number. This tends to prove that the water surface time evolution is probably experiencing a different behaviour, but it was not monitored here. Also and unfortunately, the considered velocity range studied here prevented us to go further, with higher Froude numbers. But an important modification seems to have happened. For the configurations with $D = 6$ cm, 10 cm and 14 cm at $P_0 = 0.75\,bar$, no clear trend can be extracted from the presented results. Higher velocities and depressurisation ranges enabling a better characterisation of the encountered phenomena will be studied in the near future to ascertain this observation.

4.2. Pressure impulse evolution with impact velocity

This section addresses the pressure impulse in order to verify the trend of the curves by comparing different plate diameters and the three ambient pressures.

Fig. 11 depicts the variation of the pressure impulse against the impact velocity for the four diameters in the case of the three ambient pressures. Symbols and colours are the same as the previous subsection. Looking at the pressure impulse here is also interesting because it encompasses both the maximum pressure value but also the impact duration in a single variable. From Fig. 11, one can observe that the normalised pressure impulse $I/P_0.D.V^{-1}$ value increases with the impact velocity for all the ambient pressures. For $P_0 \approx 1.015\,bar$, the points are nearly all superimposed except for $D = 3$ cm showing slightly higher values. This behaviour, already shown in Fig. 8, was attributed to the fact that, for this smaller plate size, less air could be entrapped during the impact, mechanically reducing the cushioning effect. The obtained impacts are then sharper, with less damping for the air layer, thus increasing the pressure impulse.

For $P_0 \approx 0.75\,bar$, slightly higher values can also be identified from the points with $D = 3$ cm and, to a smaller extent, $D = 6$ cm. But generally speaking, the respective impulse values are all higher than those obtained for $P_0 \approx 1.015\,bar$. And finally, for $P_0 \approx 0.5\,bar$, all the points seem to follow the same trend. But again, the respective impulse values are all higher than those obtained for $P_0 \approx 1.015\,bar$ and $P_0 \approx 0.75\,bar$. Such a behaviour was expected from the previous results and an analysis of the temporal pressure signals will give more insight into it.

Fig. 12 depicts these signals showing the peak pressure and the pressure oscillations post impact. This figure compares time signals of the pressure for $V = 1.2$ m/s as a function of the ambient pressures for the four diameters. Generally, for $D = 6$ cm, 10 cm and 14 cm, the peak slamming pressure becomes more acute for $P_0 = 0.5bar$. This can be explained by a decrease in the amount of the entrapped air compared to $P_0 = 0.75bar$ and $P_0 = 1.015\,bar$. However, the duration of the pressure impulse is decreasing as the ambient pressure decreases; i.e, the quantity of the entrapped air decreases. This behaviour was also observed numerically by Braeunig et al. (2009). The variation of the cushion effect is clearly visible in the case of $D = 14$ cm. The amplitude of the peak slamming pressure is increasing as the ambient pressure decreases, and the duration of the impact pressure is decreasing. On the other hand, for $D = 3$ cm, the amplitude as well as the duration of the pressure impulse do not vary much according to the ambient pressure.

The cushion effect is also clearly visible on post impact pressure oscillations. Indeed, as the ambient pressure decreases, the oscillations are shifted and the oscillations' periods increase. Hence, the ambient air pressure strongly influences the air cushion effect during impact. In the next section, the last stage of these signals will be evaluated in more details in order to understand the origin of the post impact pressure oscillations.

5. Spectral analysis of the pressure signal

The following section will present and discuss pressure oscillations measured just after impact and their related spectra as depicted in Fig. 13. The presented measurements are obtained for an impact velocity of $V = 1.2$ m/s. The top plots are pressure records for $P_0 =$

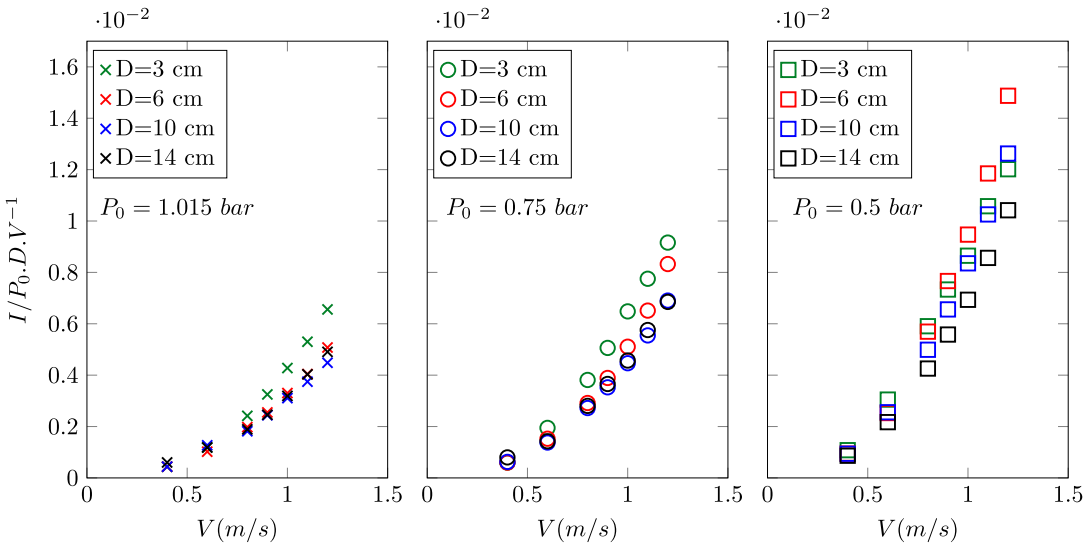

Fig. 11. Pressure impulse evolution as a function of impact velocity for different ambient pressures and different plate diameters.

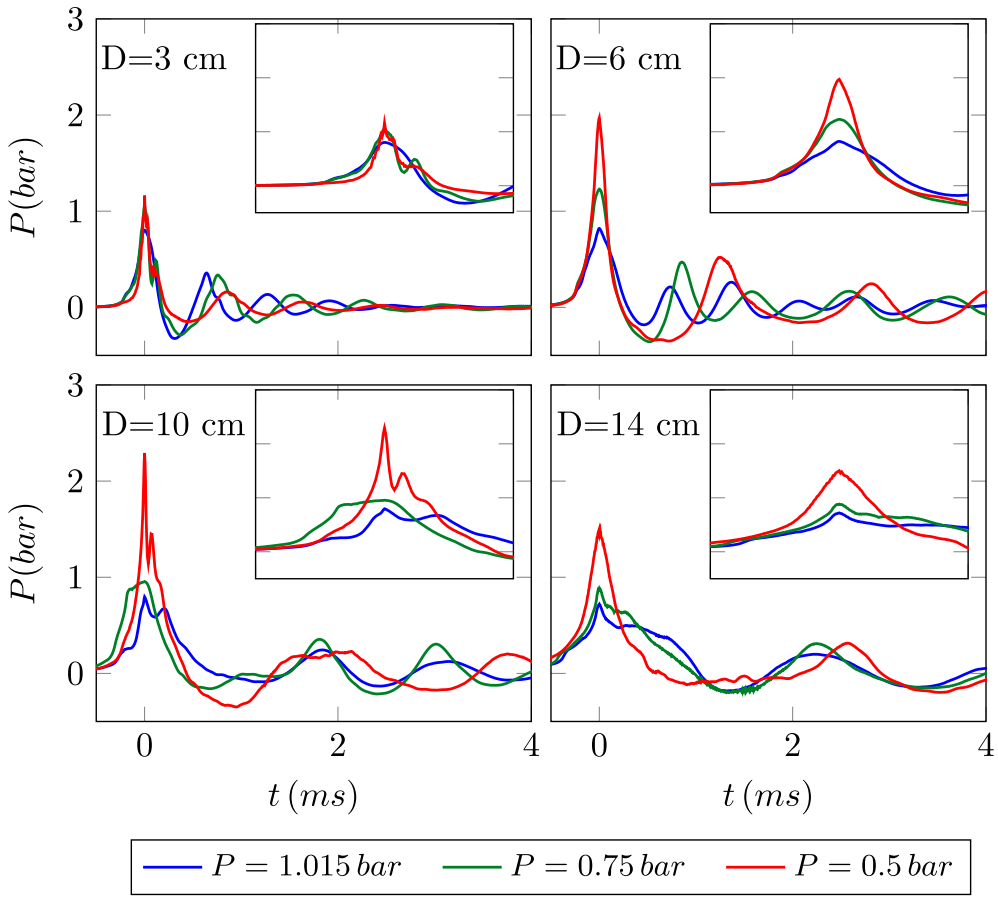

Fig. 12. Temporal pressure signals at impact velocity $V = 1.2$ m/s, for the four plates at different ambient pressures. The insert is a zoom of the peak pressure for $t \in [-0.5; 0.5]$ ms.

1.015 *bar* (Fig. 13,a), 0.75 *bar* (Fig. 13,b) and 0.5 *bar* (Fig. 13,c) and the different colours represent the different plate diameters. The bottom plots (Fig. 13d, e, f) are the corresponding Power Spectral Density (PSD). From the temporal pressure signal, one can already observe that the oscillating periods increase with the plate size. On the contrary, the influence of ambient pressure P_0 on the oscillating period is not straight forward and deeper analysis is required.

Fig. 14 shows an example of a two-dimensional representation of the pressure spectra for different impact velocities V ranging from 0.4 to 1.2 m/s and for an ambient pressure of $P_0 = 0.5bar$. Each plot of Fig. 14 corresponds to a given plate diameter D. This 2D representation is interesting in the sense that it highlights possible variation of peak frequency as a function of impact velocity V. And from the depicted plots of Fig. 14, one can clearly observe that the peak frequency is nearly constant over the whole velocity range for a given plate

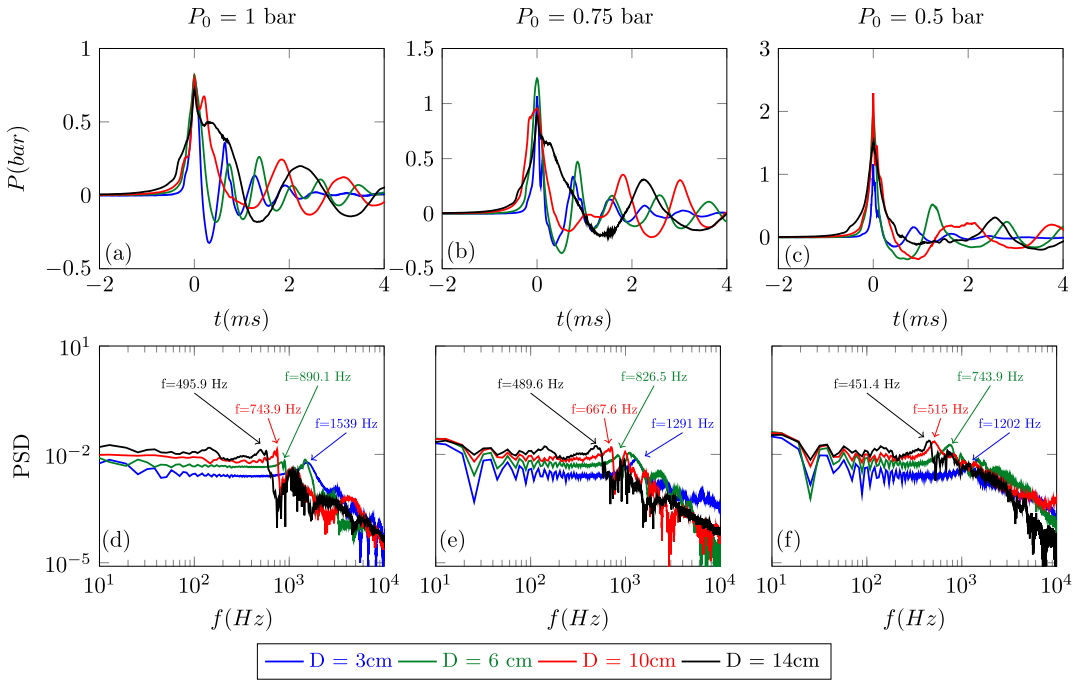

Fig. 13. Pressure oscillations versus time (top plots) and the corresponding spectra (bottom plots) impact velocity of $V = 1.2$ m/s. The reader is reminded here that the ordinate scale for the pressure value P vary with the ambient pressure P_0.

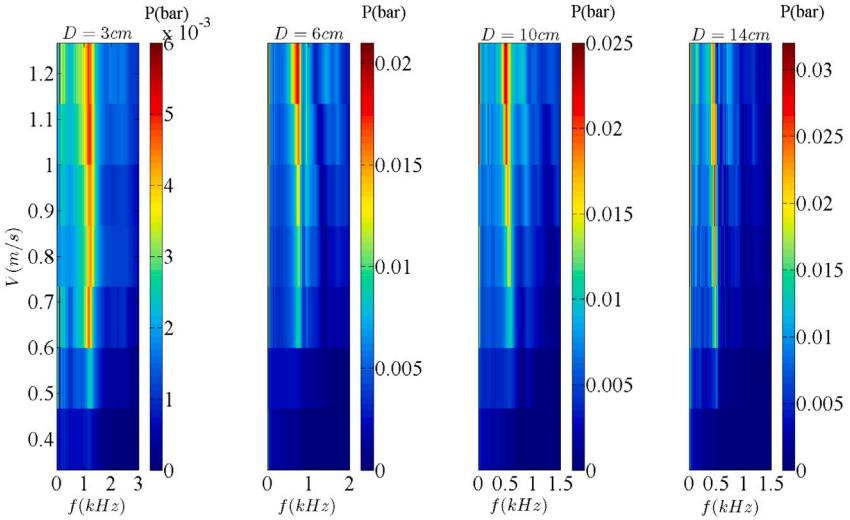

Fig. 14. A two-dimensional representation of the pressure spectra for different impact velocities V ($0.4 \leq V \leq 1.2$ m/s). Each plot corresponds to a given plate diameter D. Those results are obtained for an ambient pressure of $P_0 = 0.5bar$.

diameter D. However, the amplitude of oscillations, i.e. amplitude of the spectrum peak, increases with the impact velocity. As a matter of partial conclusion, the peak frequency does not depend on the impact velocity (for the tested velocity range of $0.4 \leq V \leq 1.2$ m/s) but may vary with respect to the plate diameter D and ambient pressure P_0.

In order to better understand the physical interpretation of obtained peak frequencies, two mechanisms can be invoked:

- an acoustic pressure wave initiated by the plate's impact and that travels in any direction in the water media and rebound on the tank walls (see the 3D scheme of Fig. 15 and Fig. 15,a),
- pressure oscillations of the entrapped air between the impinged water surface and the impacted plate (see Fig. 15,b).

For the first mechanism, the pressure wave propagation frequencies can be calculated by taking into account the tank length L, the width l and also the still water-level height h. The corresponding frequencies can basically be deduced from the following expression:

$$f = c/S, \tag{1}$$

where S either corresponds to the l, L or $2h$ and $c \approx 1450$ m/s the speed of sound in water. To the authors' belief, the sound celerity in the water c should not differ with respect to the different ambient pressure P_0. Based on the aforementioned equation, the calculated frequencies are $f = 3053$ Hz, 2762 Hz and 1686 Hz for $S = l$, L and $2h$ respectively.

The second mechanism considers repeated compression and expansion phases of the entrapped air between the impinged water surface and the impacted plate. Such a mechanism was already evoked and presented in previous studies such as in Verhagen et al. (1967), Lewison et al. (1968) and more recently by Mai et al. (2019). For this last

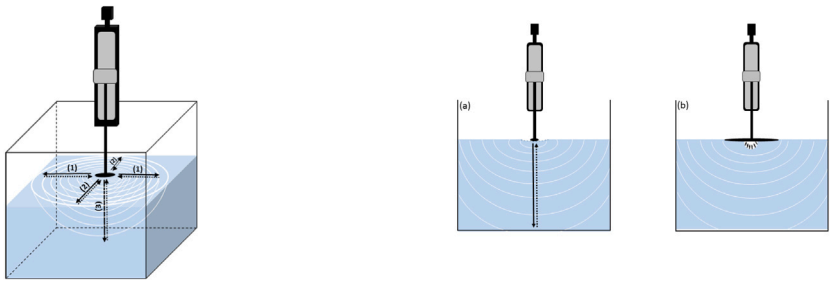

Fig. 15. Illustration of the two possible mechanisms for interpreting pressure oscillation after impact: (a) acoustic pressure wave travelling in the water media and rebounding on the tank's wall or (b) pressure oscillation of the entrapped air between the impinged water surface and the impacted plate.

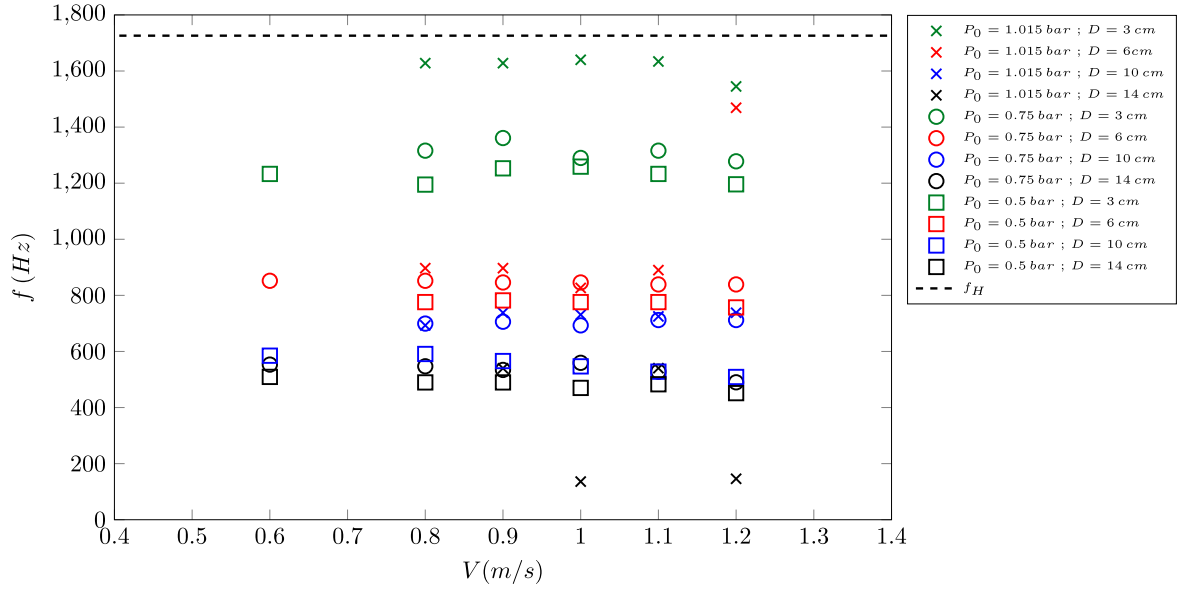

Fig. 16. Frequencies against V for different P_0 and D.

phenomenon, an estimation of the oscillation frequency is more complicated to extract and the obtained peak frequencies should depend on the plate size D and possibly the ambient pressure P_0 as the quantity of entrapped air may vary depending on P_0, hence having an influence on the bubble size and shape.

In the following, the peak frequencies obtained with the Fast Fourier Transforms will be gathered and checked to verify which of these two mechanisms is dominant. Fig. 16 compares the obtained frequencies corresponding to the largest peak, as a function of the impact velocity V, plate diameter D and ambient pressure P_0. For some isolated velocities, the peak frequency is quite different from the others for a given plate diameter and ambient pressure. However, as it can be seen on Fig. 13 several peaks are often visible and the more common frequency corresponds to the second peak in amplitude. For instance, for $D = 6$ cm at $P_0 = 1.015\,bar$ and $V = 1.2$ m/s, the highest peak is at 1469 Hz. However, the second peak is at $\approx$ 890 Hz which is the frequency of the first peak for all the other velocities. For clarity reasons only the frequencies of the highest peak are represented. The symbols and colours are the same as in the previous sections. The black dashed line represents the frequency based on the first mechanism (acoustic pressure wave in the water) calculated by taking into account pressure wave reflection at the bottom of the tank. The two other frequencies (for both vertical walls) being much higher, they were not represented here. From all the presented configurations, one can see that peak frequency generally does not vary much depending on the impact velocity V. However, and as previously indicated, peak frequency decreases by increasing the plate size. Moreover, for a given diameter, the obtained frequencies become lower by decreasing the ambient pressure.

These last two observations are consistent with the oscillatory behaviour of an air bubble immersed in the water. This configuration was studied by Minnaert and presented in its 1933's paper (Minnaert, 1933). In this document, Minnaert indicates that the natural frequency of an air bubble immersed in the water f_b could be evaluated by:

$$f_b = \frac{1}{2\pi R_b}\sqrt{3\gamma_g P_0/\rho}, \tag{2}$$

where R_b is the bubble radius, γ_g is the polytropic constant of the gas in the bubble ($\gamma_g = 1.4$ for a diatomic gas), P_0 is the ambient pressure and ρ is the water density. From Eq. (2), one can observe that the predicted frequency should slightly increase with ambient pressure P_0 and should decrease with increasing R_b. As the plate size increases, the quantity of entrapped air will also increase, leading to a larger air bubble between the impacted plate and the water surface. This is confirmed by Fig. 17 representing the peak frequencies for all cases as a function of $\sqrt{P_0}/D$. The frequencies seem to be aligned on a straight line which is consistent with the physical interpretation given by the Minnaert's equation (2).

6. Conclusions

This paper investigated the maximum impact pressures and pressure impulses for different size plates impinging a still water surface at different surroundings ambient pressures. Each experimental test was repeated 5 times to ascertain the repeatability of the obtained results. The objective of the paper was, following the work of Braeunig et al.

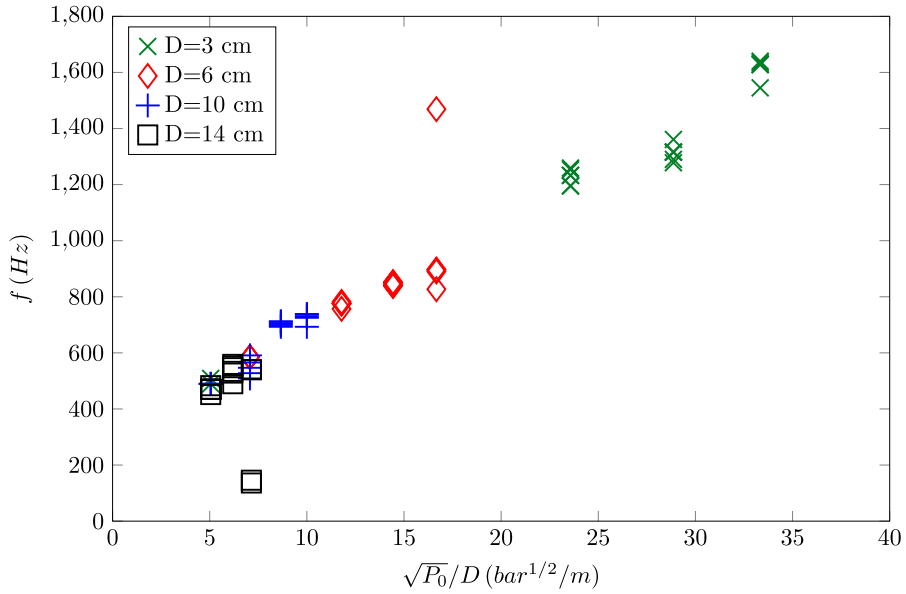

Fig. 17. Main peaks frequencies, identified on pressure signals power density spectrum, as a function of $\sqrt{P_0}/D$ as it appears in Minnaert (1933) formula for a bubble resonance.

(2009), to see whether an experimental validation of the von Karman's theory for maximum impact pressure at the very first instants of impact was possible.

A first series of measurements was made at ambient pressure, close to the atmospheric pressure. Unsurprisingly, the recorded impact pressure did not scale with the von Karman's theory and the cushioning effect of air was identified as a possible source of explanation. For all the tested configurations, the obtained maximum impact pressures and pressure impulses are consistent with the latest results in the literature. And maximum impact pressure was scaling with the square of the velocity for the studied dataset and given the range of impact velocities.

Two additional series of measurements were made at different sub-atmospheric ambient pressure, the lower being at $P_0 = 0.5\,bar$. The aim was to reduce, or even to possibly suppress, the cushioning effect by reducing the air quantity entrapped between the plate and the water surface. The obtained results always showed an increase in maximum impact pressures and pressure impulses when reducing the ambient pressure; a moderate ambient increase at $P_0 = 0.75\,bar$ and a much larger increase at $P_0 = 0.5\,bar$. This was observed except for the smaller plate with $D = 3$ cm where no significant differences were recorded. Deeper analysis showed that the maximum impact pressures were still scaling with the square of the impact velocity and a linear regression were established with respect to the Euler number. However, at the lower ambient pressure, an other physical phenomenon becomes important for plate sizes larger than $D = 3$ cm, which leads to dimensionless impact pressure evolving linearly with the Froude number. However, the velocity range tested here or the maximum depressurisation achievable with the current experimental device prevented deeper support of the obtained findings. Also, an experimental validation of the von Karman's theory for maximum impact pressure was not achieved here and this may require higher depressurisation, close to vacuum. Concerning the two tested sub-atmospheric ambient pressure configurations, a cushion effect was still observable.

The last section of this paper is dedicated to the frequency analysis of the recorded pressure signal in order to better characterise the entrapped air layer. For each tested configuration, a clear frequency was observable independent from the impact velocity but varying with the plate size, which could be related to the entrapped air volume or size. Finally, the obtained peak frequency was shown to have a similar evolution as the one identified by Minnaert (1933) for the natural frequency of an air bubble in fluid. The equation proposed by Minnaert did not fit with our results, most probably due to the fact that the experimental configurations are different. However, the evolution given by Minnaert's equation fits well with the present results and accurately predicts the variation for different plate size and ambient surrounding pressures.

For the perspectives, the authors plan to install another displacement system in order to reach higher impact velocities. Another challenge would be to develop an experimental device in order to reach lower ambient pressures. Or and more easily feasible, the possibility to carry out tests with fluids of different compressibility (e.g. methanol and hydraulic fluid) in order to highlight possible different behaviours could be more rapidly envisaged. Also, the plates being made of 10 mm thick of plain steel and the assembly rigidly mounted on the frame, the authors feel that the plate elasticity or assembly rigidity may not play a role. However, even more attention may be paid on that topic in the forthcoming work in order to avoid Fluid–Structure Interaction, as studied for instance by Truong et al. (2021) recently. And finally, a numerical study is under progress in order to complete and validate the obtained experimental findings. With such a numerical approach, larger plates together with a larger sampling of the plate sizes could be tested more easily prior to testing/validating the obtained results experimentally.

CRediT authorship contribution statement

Abdessamad Talioua: Investigation, Methodology, Resources, Formal analysis, Data curation, Visualization, Writing – original draft. **Belaïd Berkane:** Investigation, Methodology, Resources, Formal analysis, Data curation, Visualization. **Marc Batlle Martin:** Methodology, Resources, Formal analysis, Writing – review & editing. **Gaële Perret:** Conceptualization, Methodology, Resources, Formal analysis, Data curation, Writing – review & editing, Supervision, Project administration, Funding acquisition. **Grégory Pinon:** Conceptualization, Methodology, Resources, Formal analysis, Writing – review & editing, Supervision, Project administration, Funding acquisition.

Declaration of competing interest

The authors declare that they have no known competing financial interests or personal relationships that could have appeared to influence the work reported in this paper.

Acknowledgements

This work was supported in part by the European Regional Development Fund (ERDF) and the Normandy Regional Council via DIADEMAR program. A.T. acknowledges the support of DIADEMAR for the funding of his post-doc. The authors acknowledge the financial support of the French Agence Nationale de la Recherche and LabEx EMC3 through the Project PERCUSS (Grant No. ANR-10-LABX-09-01). B.B. acknowledges the support of PERCUSS and M.B.M acknowledges the Normandy Regional Council for the funding of their PhD. All the authors acknowledge the technical support of Matthieu Beaujard and Claude Houssin for their precious help during the preparation of the experimental device.

References

Bagnold, R.A., 1939. Interim report on wave-pressure research. (includes plates and photographs). J. Inst. Civ. Eng. 12 (7), 202–226. http://dx.doi.org/10.1680/ijoti.1939.14539, arXiv:https://doi.org/10.1680/ijoti.1939.14539.

Batlle Martin, M., Pinon, G., Reveillon, J., Kimmoun, O., 2021. Computations of soliton impact onto a vertical wall: Comparing incompressible and compressible assumption with experimental validation. Coast. Eng. 164, 103817.

Braeunig, J.-P., Brosset, L., Dias, F., Ghidaglia, J.-M., et al., 2009. Phenomenological study of liquid impacts through 2D compressible two-fluid numerical simulations. In: The Nineteenth International Offshore and Polar Engineering Conference. International Society of Offshore and Polar Engineers.

Bullock, G., Crawford, A., Hewson, P., Walkden, M., Bird, P., 2001. The influence of air and scale on wave impact pressures. Coast. Eng. 42 (4), 291–312.

Chuang, S.-L., 1966. Slamming of Rigid Wedge-Shaped Bodies with Various Deadrise Angles. Tech. Rep., DAVID TAYLOR MODEL BASIN WASHINGTON DC STRUCTURAL MECHANICS LAB.

Chuang, S.-L., et al., 1966. Experiments on flat-bottom slamming. J. Ship Res. 10 (01), 10–17.

Gatin, I., Liu, S., Vuković, V., Jasak, H., 2020. Finite volume method for general compressible naval hydrodynamics. Ocean Eng. 196, 106773. http://dx.doi.org/10.1016/j.oceaneng.2019.106773, URL https://www.sciencedirect.com/science/article/pii/S0029801818311958.

Guilcher, P., Oger, G., Brosset, L., Jacquin, E., Grenier, N., Le Touzé, D., 2010. Simulation of liquid impacts with a two-phase parallel SPH model. In: Proceedings of 20th International Offshore and Polar Engineering Conference. June 20-26, Bejing, China.

Hattori, M., Arami, A., Yui, T., 1994. Wave impact pressure on vertical walls under breaking waves of various types. Coast. Eng. 22 (1), 79–114. http://dx.doi.org/10.1016/0378-3839(94)90049-3, Special Issue Vertical Breakwaters. URL http://www.sciencedirect.com/science/article/pii/0378383994900493.

von Karman, T., 1929. The Impact on Seaplane Floats During Landing. National Advisory Committee on Aeronautics.

Kimmoun, O., Scolan, Y., Malenica, Š., et al., 2009. Fluid structure interactions occuring at a flexible vertical wall impacted by a breaking wave. In: The Nineteenth International Offshore and Polar Engineering Conference. International Society of Offshore and Polar Engineers.

Lewison, G., Maclean, W., et al., 1968. On the cushioning of water impact by entrapped air. J. Ship Res. 12 (02), 116–130.

Lu, X., Cherfils, J.-M., Pinon, G., Rivoalen, E., Kimmoun, O., Brossard, J., 2021. SPH numerical computations of wave impact onto a vertical wall with experimental comparisons. C. R.. Méc. 349 (1), 117–143. http://dx.doi.org/10.5802/crmeca.72.

Lugni, C., Brocchini, M., Faltinsen, O.M., 2010a. Evolution of the air cavity during a depressurized wave impact. II. The dynamic field. Phys. Fluids 22 (5), 056102. http://dx.doi.org/10.1063/1.3409491, arXiv:https://doi.org/10.1063/1.3409491.

Lugni, C., Miozzi, M., Brocchini, M., Faltinsen, O., 2010b. Evolution of the air-cavity during a depressurized wave impact. Part I: The kinematic flow field. Phys. Fluids 22, http://dx.doi.org/10.1063/1.3407664.

Ma, Z., Causon, D., Qian, L., Mingham, C., Ferrer, P.M., 2016. Numerical investigation of air enclosed wave impacts in a depressurised tank. Ocean Eng. 123, 15–27. http://dx.doi.org/10.1016/j.oceaneng.2016.06.044, URL http://www.sciencedirect.com/science/article/pii/S0029801816302347.

Ma, Z.H., Causon, D.M., Qian, L., Mingham, C.G., Gu, H.B., Ferrer, P.M., 2014. A compressible multiphase flow model for violent aerated wave impact problems. Proc. R. Soc. A 470 (2172), 20140542. http://dx.doi.org/10.1098/rspa.2014.0542, arXiv:https://royalsocietypublishing.org/doi/pdf/10.1098/rspa.2014.0542. URL https://royalsocietypublishing.org/doi/abs/10.1098/rspa.2014.0542.

Mai, T., Mai, C., Raby, A., Greaves, D., 2019. Aeration effects on water-structure impacts: Part 1. drop plate impacts. Ocean Eng. 193, 106600.

Minnaert, M., 1933. XVI. On musical air-bubbles and the sounds of running water. Lond. Edinb. Dublin Philos. Mag. J. Sci. 16 (104), 235–248.

de Rouville, A., Besson, P., Petry, P., 1938. État actuel des études internationales sur les efforts dus aux lames.

Stevenson, T., 1840. The design and construction of harbours: A treatise on maritime engineering. In: Cambridge Library Collection - Technology, Cambridge University Press, http://dx.doi.org/10.1017/CBO9780511997020.

Truong, D.D., Jang, B.-S., Ju, H.-B., Han, S.W., 2021. Prediction of slamming pressure considering fluid-structure interaction. Part II: Derivation of empirical formulations. Mar. Struct. 75, 102700. http://dx.doi.org/10.1016/j.marstruc.2019.102700, URL https://www.sciencedirect.com/science/article/pii/S0951833919304150.

Verhagen, J., et al., 1967. The impact of a flat plate on a water surface. J. Ship Res. 11 (04), 211–223.

Wood, A., 1941. A Textbook of Sound: Bell. London.

Zhao, R., Faltinsen, O., Aarsnes, J., 1997. Water entry of arbitrary two-dimensional sections with and without flow separation. In: Twenty-First Symposium on Naval Hydrodynamics. The National Academies Press, http://dx.doi.org/10.17226/5870.

Zhu, L., 1995. Structural response of ship plates in slamming-drop test results and analysis. UNIVERSITY of GLASGOW DEPARTMENT of NAVAL ARCHITECTURE and OCEAN ENGINEERING-REPORTS-NAOE.